

Results from the RICE experiment: Limits on the ultra-high energy neutrino flux

D. Seckel¹, G. Spiczak¹, J. Adams², S. Seunarine², G. M. Frichter³, C. Allen⁴, A. Bean⁴, D. Besson⁴, D. J. Box⁴, R. Buniy⁴, E. Copple⁴, D. McKay⁴, J. Ralston⁴, S. Razzaque⁴, D. W. Schmitz⁴, and I. Kravchenko⁵

¹Bartol Research Institute, U. of Delaware, Newark DE 19716

²Department of Physics and Astronomy, Private Bag 4800, U. of Canterbury, Christchurch, New Zealand

³Florida State University, High Energy Physics, Tallahassee FL 32306-4350

⁴University of Kansas Dept. of Physics and Astronomy, Lawrence KS 66045-2151

⁵Massachusetts Institute of Technology Lab. for Nuclear Science, Cambridge, MA 02139

Abstract. The RICE experiment (Radio Ice Cherenkov Experiment) at the South Pole, co-located with the AMANDA experiment, aims to detect ultra-high energy (UHE) electron neutrinos ($E_\nu > 10^{15}$ eV) by detection of the long-wavelength Cherenkov Radiation (CR) signal resulting from neutrino-induced showers in cold Polar ice: $\nu_e + N \rightarrow e + N'$. We present upper limits on the UHE ν_e flux based on analysis of August, 2000 data.

1 Introduction

The RICE experiment has similar goals to the larger AMANDA experiment - both seek to measure ultra-high energy (UHE) neutrinos by detection of Cherenkov radiation produced by $\nu_l + N \rightarrow l + N'$. Whereas AMANDA is optimized for detection of penetrating muons resulting from $\nu_\mu + N \rightarrow \mu + N'$, RICE is designed to detect compact electromagnetic cascades initiated by e^+ / e^- : $\nu_e + N \rightarrow e^\pm + N'$. As the cascade develops, atomic electrons in the target medium are swept into the forward-moving shower, resulting in a net charge on the shower front of $Q_{tot} = E_s e / 4$; E_s is the shower energy in GeV (Razzaque, 2001).

Such cascades produce broadband Cherenkov radiation – for wavelengths much larger than the transverse dimensions of the shower front ($2r_{Moliere}$, or ≈ 26 cm in ice), the emitting region approximates a point charge of magnitude Q_{tot} . At these (RF) wavelengths, the net CR produced by the shower front can therefore be considered coherent (Askaryan, 1961). By contrast, at optical frequencies, the wavelength is short compared to the shower size, thus the electric field contributions of individual charges in the shower add incoherently. The experimental sensitivity in the long-wavelength radio regime is further enhanced by the very long attenuation length for cold polar ice ($\alpha_{atten}^{1\text{GHz}} \sim 1$ km). Although estimates vary, one calculation finds (Price, 1995) that somewhere in the range $1 \text{ PeV} < E_{\nu_e} < 10 \text{ PeV}$, radio techniques become

competitive with PMT-based techniques.

The RICE experiment presently consists of an 18-channel array of radio receivers (“Rx”), scattered within a $200 \text{ m} \times 200 \text{ m}$ cube, at 100-300 m depths. The signal from each antenna is boosted by a 36-dB in-ice amplifier, then carried by coaxial cable to the surface observatory, where the signal is filtered (suppressing noise below 200 MHz), re-amplified (either 52- or 60-dB gain), and fed into a CAMAC crate. After initial discrimination (using a LeCroy 3412E discriminator), the signal is routed into a NIM crate where the trigger logic resides. A valid trigger signal initiates readout of receiver waveforms, as recorded on HP54542 digital oscilloscopes. Also deployed are three large TEM surface horn antennas which are used to veto surface-generated noise.

2 Expected Signal Strength

Calculations of the radio-frequency electric field characteristics produced by a neutrino-induced shower are discussed elsewhere (Razzaque, 2001). The expected signal strength found from a GEANT-based simulation is presented in Figure 1 as a function of observation angle for different frequency components. The simulation is performed in the Fraunhofer approximation (large observation distance).

Two shower simulations and electric field calculations have been compared (the GEANT-based code and code written by by Zas, Halzen and Stanev (Zas, 1992)). They differ by $\sim 30\%$ in the peak electric field magnitude. For the flux upper limits calculated here, we conservatively choose the weaker GEANT prediction. To ensure that the GEANT-based simulation is giving reasonable results, simulation predictions for Moliere radius, radiation length, critical energy, total track-length, particle yields as a function of shower depth, and dE/dx as a function of particle momentum energy are all compared to data, where possible, for a variety of media. In all cases, the simulation agrees reasonably well with expectations from data.

Correspondence to: Dave Besson (dbesson@ku.edu)

The shower detection efficiency is determined by a de-

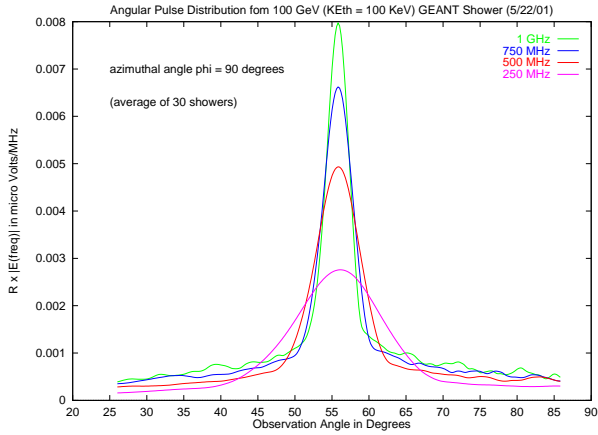


Fig. 1. Electric field strength vs. observation angle, for four different frequencies. Results are taken from GEANT shower simulations. As expected, the width of the coherence region sharpens with increasing frequency (decreasing wavelength).

tailed Monte Carlo (MC) of the RICE experiment. Crudely, the MC can be divided into three parts. The first generates and propagates the radio CR, and results in an electric field $\mathbf{E}_i(t)$ at each antenna i . The second part simulates the response of each antenna, and propagates the antenna output signals through our electronics to form an input voltage $V_i(t)$ for each channel of the DAQ hardware. The third generates the event trigger, and tests against the various veto conditions applied in hardware and software.

3 Event Triggers and Source Reconstruction

A valid event trigger is defined when any one of three criteria is satisfied in a time window of $1.2 \mu\text{s}$: a) ≥ 4 under-ice antennas register signals above threshold, b) ≥ 1 under-ice antenna registers a signal above threshold in coincidence with a high-amplitude SPASE event, c) ≥ 1 under-ice antenna registers a signal above threshold in coincidence with a 30-fold PMT AMANDA-B event. To reject background noise, there are two primary ways that events can be vetoed: a) one of the surface horn antennas registers a signal in coincidence with any of the above three trigger criteria being satisfied, or b) the timing sequence of hits in the under-ice antennas is determined to be consistent (in software) with the sequence expected from surface-generated backgrounds.

If any of the above trigger criteria are satisfied and the event has not been vetoed, the time of each hit above threshold (as recorded by LeCroy 3377 TDC), and also an $8 \mu\text{s}$ buffer of data for that channel (stored in an HP54542A digital oscilloscope at 1 GSa/s) is written to disk. At present, raw trigger rates (before veto) are adjusted to be typically 1 Hz; typical data-taking rates after the veto are $0.01 - 0.1$ Hz.

Event and source reconstruction is based on our knowledge of the array geometry, ice properties and thus the expected times a wave-front propagates from the source to any given receiver location. Knowing the time differences δt_{ij}

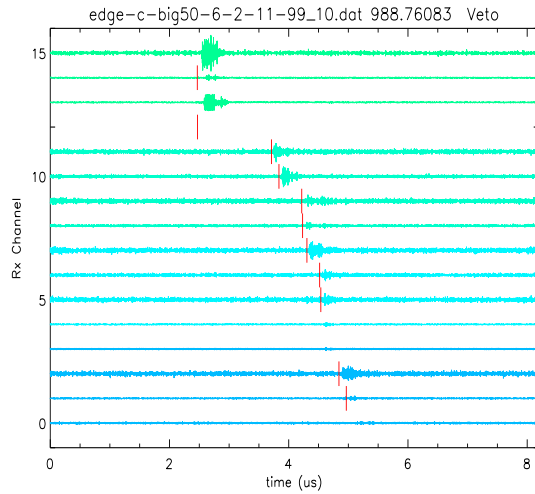


Fig. 2. Voltage(t) traces for a typical event. Receiver channels are ordered (from top to bottom) by distance from the surface. Recorded TDC times (|) are superimposed on the digital oscilloscope traces.

between all pairs (i, j) of hit antennas, we perform χ^2 minimization to find the source location and source direction. For full reconstruction this method requires at least four antennas to be hit (i.e., $3\delta t_{ij}$ values). The event reconstruction is described in more detail in a companion paper (Seckel, 2001).

A typical event, as recorded in the digital oscilloscopes, is displayed in Figure 2. Shown are the oscilloscope traces corresponding to 15 receiver channels. The arrival of the pulse in each channel is evident from the figure; since the channels are ordered by their relative distance from the surface observatory, one observes in this event the clear signature of surface-generated noise sweeping down through the array from top to bottom. The characteristic pattern observed in this figure satisfies veto criterion b) as enumerated above (note that we save a fraction of the veto events for future analysis).

Contributions to the timing uncertainty come from several sources, including differences in signal propagation velocity in the ice due to variations in the dielectric constant with depth, differences in signal propagation speed within the different analog cables being used, differences in cable lengths, and receiver (and transmitter) location uncertainties. Typical resolution on the risetime of a transient signal is of order 10-20 ns (see, e.g. Figure 2). With the timing calibration as described elsewhere (Seckel, 2001), we then perform source reconstruction on neutrino candidate data. Sources are reconstructed in exactly the same fashion as described for the timing calibration based on transmitter studies. We have chosen the August, 2000 dataset for our initial analysis due to the stability of the data acquisition system during that time.

Preliminary software criteria are imposed to quickly identify and flag obvious non-neutrino events in our data set. Events are rejected if they fail a software threshold cut (we require that 4 hits contain signals exceeding $5\sigma_V$, where σ_V

is the rms voltage for that channel) or if they show evidence for double pulses (not expected for true neutrino events). From our study of unbiased events, the random occupancy in each channel has been determined to be extremely small ($\ll 1\%$ per channel); the possibility of four antennas randomly firing to create an event trigger which “shadows” a true neutrino event is correspondingly negligible. After rejecting events which give an event vertex above the surface (either using all $5\sigma_V$ hits, or by repeated fitting after successively eliminating each of the four hits that give the largest χ^2 contribution to the fit vertex), twenty events are retained for further consideration. These events are then hand-scanned; the majority of these events are background events containing single samples from the oscilloscope trace that exceed the software threshold. Such fluctuations are inconsistent with the characteristic ringing expected for an antenna responding to an impulse (ns-duration) Cherenkov electric field. Pending complete analysis of the full RICE dataset taken since Jan. 1999, it remains to be seen whether these events are the result of some instrumental effect, some transient background, or some other non-signal effect. At this stage, no amplitude information has been explicitly used to further constrain the event sample. Event selection criteria and the effect of all cuts are shown in Table 1. The efficiency for all our event selection requirements is determined from Monte Carlo simulation to be $\sim 85\%$.

Total triggers taken	1,156,774
Surface vetoes eliminated online	1,143,271
Total triggers analyzed	13503
Events passing $4 \times 5\sigma_V$ cut	73
Events passing double-pulse cut, with $Z < 0$	20
Events remaining after scanning	2

Table 1. Summary of analysis of August, 2000 data.

Our triggers in the analyzed dataset are therefore dominated by surface-generated transient noise backgrounds or random thermal noise hits; no clear neutrino candidates have been observed. The signal rate expected for other naturally occurring processes is almost negligible. For example, it has been suggested that penetrating muons from extensive air showers could produce sporadic showers from hard bremsstrahlung. With our threshold and effective volume, the rate for this process is expected to be less than 0.1 event per year (Frichter, 1998). Although neutrino searches are therefore essentially background free, it is unfortunate that we do not have a naturally occurring calibration “beam” for RICE.

To calculate the neutrino flux, the effective volume V_{eff} must be determined. Given the settings for the current RICE discriminator thresholds, and folding in known experimental circuit gains and losses (Seckel, 2001), V_{eff} is calculated as a function of incident neutrino energy (Figure 3). In the figure, the uppermost black curve corresponds to the effective volume in which only one receiver must be hit, with a discriminator threshold corresponding to thermal noise. The closely spaced curves correspond to more realistic cases requiring $n=4, 5, 6, \dots$ antennas hit, with our current discrimina-

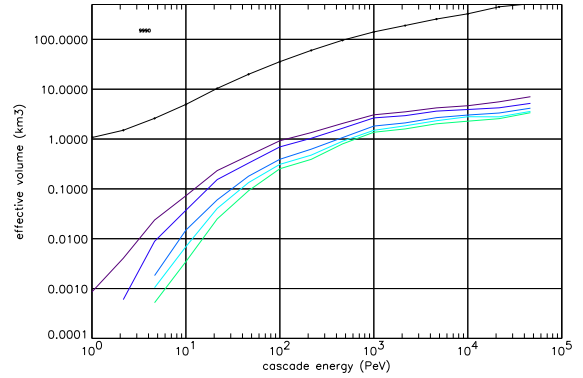


Fig. 3. Calculated effective volume, as a function of energy. The curves shown correspond to various assumptions about the experimental thresholds. Black (top) curve corresponds to the effective volume probed by an ideal, 1 GHz bandwidth radio receiver, coupled to a lossless, ideally coupled signal transmission system. Magenta, purple, blue, cyan, and green curves correspond to the effective volume probed with current RICE antennas, requiring that 4, 5, 6, 7 or 8 antennas, respectively, register a signal exceeding our currently set voltage thresholds. The current RICE trigger requires a 4-hit coincidence, and therefore corresponds to the magenta curve.

tor thresholds. The uppermost of the closely-spaced curves ($n=4$) corresponds to our current experimental configuration. For $E_\nu=10(100)$ PeV, our effective volume is $\sim 0.1(1) km^3$.

Knowing the total livetime for the August, 2000 dataset (360.1 hrs), the effective volume, and based on the two candidates which have not yet been eliminated from consideration, we calculate an upper limit on the incident ν_e flux, as a function of incident energy (Figure 4). In the figure,

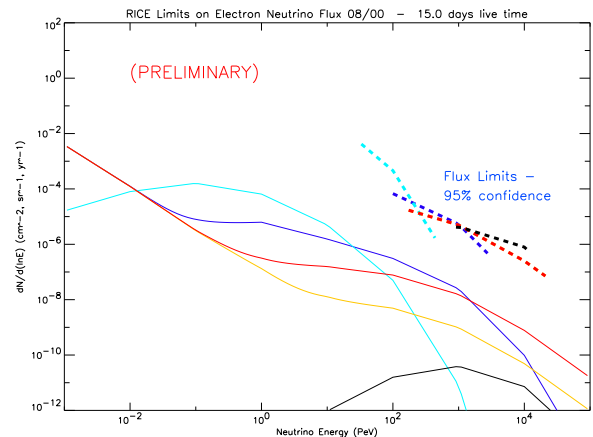


Fig. 4. Neutrino flux model predictions (solid) and corresponding RICE calculated upper limits (95% confidence level; dashed), as a function of neutrino energy.

the predictions, shown as solid lines, correspond to (in order of descending flux, as measured at 1 PeV): light blue

= Stecker & Salamon (Stecker, 1995), violet = Protheroe (Protheroe, 1994), red = Mannheim (B) (Mannheim, 2001), gold = Mannheim (A) (Mannheim, 1993), black = Yoshida et al. GZK-model (Yoshida, 1998). Dashed lines represent our current upper limits for the Stecker & Salamon, Protheroe, and Mannheim (B) models (from left to right), based on analysis of the August, 2000 data only. It is important to note that, since we have not done an energy measurement of signals, the physical quantity of interest is only the integral under the dashed line, which gives the integrated upper limit on the total neutrino flux - the shape of the curve is intended to only indicate how the sensitivity of the RICE array varies with energy and tracks a given flux model. We are currently 1-2 orders of magnitude above model predictions.

Alternately, we can plot our upper limits for different values of spectral index γ , assuming an incident neutrino energy spectrum: $dN/dE_\gamma \sim E^{-\gamma}$. These are shown in Figure 5, for a range of γ values. Here, the dashed lines cover the region for which our sensitivity is maximal given the assumed incident neutrino spectrum; the integral under the dashed line corresponds to our upper limit. As the spectral index increases, our sensitivity is pushed to lower energy regions.

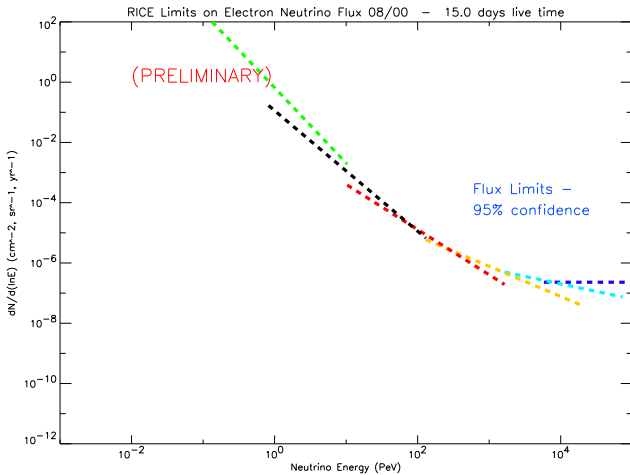


Fig. 5. RICE calculated upper limits (95% confidence level) on neutrino flux assuming $dN/dE \sim E^{-\gamma}$ input spectrum, with the spectral index varying from $\gamma=3.5$ to $\gamma=1.0$, in increments of $\Delta\gamma=0.5$ (from left to right).

4 Future Prospects and Plans

We have used only August, 2000 data for the results presented in this analysis. Data taken from Jan., 1999 - June, 2001 has yet to be fully analyzed; analysis of those data (corresponding to an order of magnitude more livetime than what we have discussed in the current analysis) should be a straightforward extension of this analysis, although it requires careful consideration of the effect of changing thresholds, changes to hardware, etc. Although our energy thresh-

old and effective volume may be too small to detect an appreciable flux of atmospheric neutrinos, in principle, many other AMANDA-accessible analyses are also accessible to RICE (monopole detection (Wick, 2000), studies of neutrinos coincident with GRB's, etc.).

Further improvement in the current array can be achieved by: a) deployment of additional receiver modules, b) improvement of signal transmission technology (low-loss optical fiber, e.g., vs. our current coaxial cable), c) improvement of signal collection technology (e.g., use of the same type of waveform digitizers currently being employed under-ice by AMANDA), and d) stronger (hardware) rejection of surface backgrounds. In the future, RICE plans to continue to take advantage of drilling opportunities presented by AMANDA and/or ICECUBE deployment to extend the size of the RICE array. Ideally, RICE modules would be deployed independently, in custom-made holes spaced at distances approximately 2-4 times larger than current holes. Such dedicated deployment would also avoid possible backgrounds presented by AMANDA cables and hardware.

Acknowledgements. We gratefully acknowledge the logistical support of the AMANDA Collaboration, the National Science Foundation Office of Polar Programs, the University of Kansas, the University of Canterbury Marsden Grant, and the Cottrell Research Corporation. We also thank the winterovers who staffed the experiment during the last two years at the South Pole (Xinhua Bai, Darryn Schneider and Steffen Richter). Very useful conversations with Peter Gorham, Jaime Alvarez-Muñiz, and David Saltzburg are also appreciated and acknowledged. We thank Igor Zheleznykh and Alexei Provorov of the Moscow Institute of Nuclear Research for design and initial construction of the TEM horn antennas currently used in our surface veto.

References

- Razzaque, S. *et al.*, these proceedings. See also G. Frichter, D. McKay and J. P. Ralston, "On Radio Detection of Ultra-High Energy Neutrinos in Antarctic Ice," *Physical Review D*, **53**, 1684 (1996)
- Askaryan, G. A., *Zh. Eksp. Teor. Fiz.* **41**, 616 (1961), and Askaryan, G. A., *Soviet Physics JETP* **14**, 441 (1962).
- Price, P. B., astro-ph/951011, (1995), and *Astropart. Phys.* **5**, 43, (1996).
- Seckel, D. *et al.*, these proceedings.
- Frichter, G., reported at the UCI ICECUBE Workshop, UC, Irvine, 1998.
- F. W. Stecker and M. H. Salamon, astro-ph/9501064.
- A. P. Szabo and R. J. Protheroe, *Astropart. Phys.* **2**, 375 (1994); R. J. Protheroe and A. P. Szabo, *Phys. Rev. Lett.* **69**, 2285 (1992).
- K. Mannheim, astro-ph/9306005, *Phys. Rev. D* **48** (1993) 2408-2414
- K. Mannheim, R. Protheroe, and J. Rachen, astro-ph/9812398, and *Phys. Rev. D* **63** (2001) 023003
- S. Yoshida, G. Sigl, and S. Lee, hep-ph/9808324, *Phys. Rev. Lett.* **81** (1998) 5505-5508, and G. Sigl, S. Lee, P. Bhattacharjee, and S. Yoshida, hep-ph/9809242, *Phys. Rev. D* **59** (1999) 043504
- Zas, E., *et al.*, *Phys. Rev. D* **45**, 362 (1992)
- S. D. Wick *et al.*, astro-ph/0102002, and astro-ph/000123, submitted to *Astro. Part. Phys.*